Assessment of Ultra-Tightly Coupled GNSS/INS Integration System towards Autonomous Ground Vehicle Navigation Using Smartphone IMU

Yiran Luo[1,2,3,4*], Chunyang Yu[4], Bing Xu[5], Jian Li[1,2,3], Guang-Je Tsai[6], You Li[4], and Naser El-Sheimy[4]

[1]Radar Research Lab, School of Information and Electronics, Beijing Institute of Technology, Beijing 100081, China
[2]Key Laboratory of Electronic and Information Technology in Satellite Navigation (Beijing Institute of Technology), Ministry of Education, Beijing 100081, China
[3]Beijing Institute of Technology Chongqing Innovation Center, Chongqing, 401120, China
[4]Department of Geomatics Engineering, University of Calgary, Calgary, AB T2N 1N4, Canada
[5]Interdisciplinary Division of Aeronautical and Aviation Engineering, The Hong Kong Polytechnic University, Kowloon, Hong Kong, China
[6]Dept. of Geomatics Engineering, National Cheng-Kung University, No. 1, Daxue Road, East District, Tainan, Taiwan
[*]Email address: yirancoffee@bit.edu.cn

***Abstract*—An ultra-tightly coupled (UTC) GNSS/INS integration navigation system is established and researched for the autonomous ground vehicle navigation based on the consumer-level inertial measurement unit (IMU). The used IMU is chosen from a smartphone in this work. The proposed integration architecture is tested with a GNSS software-defined receiver (SDR) using the vector tracking (VT) technique. The UTC integration system which is measured through both GNSS measurements and the IMU data is an upgraded version of the vector tracking technique. Meanwhile, the performances of both the integration solutions and the GNSS solutions can be improved by such advanced technology. An extremely challenging environment is chosen to verify the navigation performance. The loosely coupled (LC) GNSS/INS integration navigation system using the vector GNSS SDR and a commercial U-Blox GNSS receiver are also tested in the same scenario as comparisons. The field test results demonstrate that the proposed ultra-tight coupling algorithm can enhance the availability of the navigation solutions.**

***Index Terms*—global navigation satellite system (GNSS), ultra-tightly coupled GNSS/INS integration, vector tracking, consumer-level IMU, ground vehicle navigation**

I. Introduction

With the construction of the global positioning system (GPS) from the United States in 1970s, the application of the GPS/inertial navigation system (INS) integration technology began to rise. In 1996, Spilker firstly presented the concepts of vector delay lock loop (VDLL) which should be the prototype of the vector tracking structure for the GNSS receiver design [1]. In the same year, the deep integration was firstly presented by Draper Laboratory [2]. In 2006, the researchers at the University of Calgary provided the analysis on the differences among the ultra-tight coupling systems using different Kalman filters to estimate signal tracking errors of the GPS receiver in a GPS/INS integration system [3]. Lashley from Auburn University exploits a vector delay/frequency lock loop (VDFLL) to track signals in the Matlab software GPS receiver in his doctoral thesis [4]. For the stand-alone GNSS receiver design, some advanced techniques have been proposed to deal with the GNSS signal in severe situations. The fractional Fourier transform has been proved that it is promising to process the weak and accelerated high-dynamic GNSS signals [5]–[7]. The vector tracking is also one of the most efficient ways to overcome the issues that the challenging GNSS signals will be faced with [8]–[10]. In recent times, the ultra-tightly coupled (UTC) GNSS/INS architecture is still attracting the attentions of the researchers and being enhanced with different methods. A new UTC GNSS/INS architecture based on a phased array antenna is introduced and discussed by the researchers [11]. The consumer-level sensors are currently playing an important role in many practical applications, e.g., unmanned aerial vehicle (UAV) for indoor navigation [12], autonomous ground vehicle navigation [13], and the seamless indoor/outdoor navigation [14], etc. A consumer-level IMU, which is integrated in the smartphone, is used here to be combined with the GNSS receiver. An UTC GNSS/INS integration system based on this IMU is established, and its performance will be assessed in an extremely GNSS-challenging environment.

This work aims to compare the navigation performance using the VT-based standalone GNSS receiver with the one aided by the UTC GNSS/consumer-level IMU technique. Most of the previous research works have focused on the comparisons in terms of different integration architectures, e.g., loosely coupled (LC) and tighly coupled (TC) integration methods, or in terms of different vector tracking algorithms. Two main contributions have been made relying on this research. At first, it has proved that even if the very low-cost consumer-level IMU has the potential to rug ultra-tight coupling GNSS receiver in comparison with the vector tracking merely applied to the standalone receiver. Secondly, both the vector tracking and the ultra-tight coupling can significantly improve the

receiver's robustness in an extremely challenging environment. Hence, it is possible to provide a general guide for the wide and rapidly increased GNSS commercial market. More specifically, the GNSS receiver availability has the potential to be significantly improved at the cost of just very few extra hardware expenses.

II. EKF Model for GNSS/INS Integration

In this section, the extended Kalman filter (EKF) model for the proposed ultra-tight coupling algorithm will be discussed.

A. States and Dynamic Matrix

The state vector is modeled in the earth-centered earth-fixed (ECEF) coordinate frame (e-frame), which is given by

$$\delta \mathbf{x}_k^e = \left[(\delta\psi^e)^{\mathrm{T}}, (\delta\mathbf{v}^e)^{\mathrm{T}}, (\delta\mathbf{r}^e)^{\mathrm{T}}, (\delta\mathbf{b}_g)^{\mathrm{T}}, (\delta\mathbf{b}_a)^{\mathrm{T}} \right]_k^T \quad (1)$$

where k denotes the epoch number, $\delta\psi^e$ denotes the state vector of the attitude error; $\delta\mathbf{v}^e$ represents the state vector of velocity error; $\delta\mathbf{r}^e$ is the position error vector; $\delta\mathbf{b}_g$ and $\delta\mathbf{b}_a$ stand for the state vectors of gyro bias error and accelerometer bias error, respectively. Then, the dynamic matrix in ECEF frame is given by [15]

$$\mathbf{F} = \begin{bmatrix} -\mathbf{\Omega}_{ie}^e & \mathbf{0}_3 & \mathbf{0}_3 & \hat{\mathbf{C}}_b^e & \mathbf{0}_3 \\ \mathbf{F}_{21}^e & -2\mathbf{\Omega}_{ie}^e & \mathbf{F}_{23}^e & \mathbf{0}_3 & \hat{\mathbf{C}}_b^e \\ \mathbf{0}_3 & \mathbf{I}_3 & \mathbf{0}_3 & \mathbf{0}_3 & \mathbf{0}_3 \\ \mathbf{0}_3 & \mathbf{0}_3 & \mathbf{0}_3 & \mathbf{0}_3 & \mathbf{0}_3 \\ \mathbf{0}_3 & \mathbf{0}_3 & \mathbf{0}_3 & \mathbf{0}_3 & \mathbf{0}_3 \end{bmatrix} \quad (2)$$

with

$$\mathbf{F}_{21}^e = \left[-\left(\hat{\mathbf{C}}_b^e \hat{\mathbf{f}}_{ib}^b \right) \times \right], \quad \mathbf{F}_{23}^e = -\frac{2\hat{\gamma}_{ib}^e}{r_s\left(\hat{L}_b\right)} \frac{(\hat{\mathbf{r}}^e)^T}{|\hat{\mathbf{r}}^e|} \quad (3)$$

where $(\cdot)\times$ denotes the operator of the skew-symmetric matrix; $\mathbf{\Omega}_{ie}^e$ is the skew-symmetric matrix of the earth-rotation vector; $\hat{\mathbf{C}}_b^e$ represents body-to-earth-frame coordinate transformation matrix in current epoch; $\hat{\mathbf{f}}_{ib}^b$ is the measurement vector of the accelerometer; $\hat{\gamma}_{ib}^e$ represent the gravitational acceleration vector in the ECEF-frame axes. $r_s\left(\hat{L}_b\right)$ stands for the geocentric radius at the surface which is a function of latitude, $\hat{L}_b$ [15]. Finally, the dynamic system matrix should be transferred to the transition matrix, $\mathbf{\Phi}^e$, to be implemented in a practical system. It is approximated as

$$\mathbf{\Phi}_{k+1,k}^e \approx \mathbf{I}_{15} + \tau\mathbf{F}_k + \frac{\tau^2}{2!}(\mathbf{F}_k)^2 + \frac{\tau^3}{3!}(\mathbf{F}_k)^3 + \cdots \quad (4)$$

where $\mathbf{I}_m$ denotes the identity matrix and the subscript m is the dimension; τ is the update interval of the navigation system.

B. Observation Matrix

The observation vector is

$$\delta\mathbf{z}^e = \left[\begin{bmatrix} \tilde{x}_I - \tilde{x}_G \\ \tilde{y}_I - \tilde{y}_G \\ \tilde{z}_I - \tilde{z}_G \end{bmatrix}^T, \begin{bmatrix} \tilde{\dot{x}}_I - \tilde{\dot{x}}_G \\ \tilde{\dot{y}}_I - \tilde{\dot{y}}_G \\ \tilde{\dot{z}}_I - \tilde{\dot{z}}_G \end{bmatrix}^T \right]^T \quad (5)$$

where the subscript I denotes the measurements in terms of the INS, while G represents the counterparts in terms of the GNSS receiver. It is known that $\mathbf{r}^e = [x, y, z]^T$ and $\mathbf{v}^e = [\dot{x}, \dot{y}, \dot{z}]^T$ are the positions and velocities in the e-frame. The associated observation matrix is given by

$$\mathbf{H}^e = \begin{bmatrix} \mathbf{0}_{6\times3} & \begin{bmatrix} 0 & 1 \\ 1 & 0 \end{bmatrix} \otimes \mathbf{I}_3 & \mathbf{0}_{6\times6} \end{bmatrix} \quad (6)$$

where $\otimes$ stands for the Kronecker product operator.

C. Noise Covariance Matrices

The IMU data used in this work are from the smartphone of Huawei Mate 9, i.e., LSM6DSM produced by STMicroelectronics. When the small propagation interval, i.e., $\Delta t < 0.2$ seconds, is contained in the algorithm, the process covariance matrix can be approximated as [15]

$$\mathbf{Q} \approx \left\{ diag\left[\sigma_{gb}^2, \sigma_{ab}^2, 0, \sigma_{gd}^2, \sigma_{ad}^2\right] \otimes \mathbf{I}_3 \right\} \times \Delta t \quad (7)$$

where $diag\left[\cdot\right]$ denotes the operator of the diagonal matrix, σ_{gb}, σ_{ab}, σ_{gd} and σ_{ad} represent the standard deviation (STD) of gyro bias error, accelerometer bias error, gyro drift error, accelerometer drift error, respectively; Δt is the update interval. The noise distribution of the observation covariance matrix is primarily dependent on the quality of the GNSS solutions, i.e., positioning and velocity results. Such matrix is formed with empirical values in this work and it is given by

$$\mathbf{R} = diag\left[5^2, 0.1^2\right] \otimes \mathbf{I}_3 \quad (8)$$

D. GNSS/INS Integration Solutions

The state variables can be estimated and updated using the KF recursive formula [16]. Then, the integration results will be fed back to the carrier numerically controlled oscillator (NCO) such that the bandwidth of the tracking loop can be optimized. Thus, the Doppler frequency of jth channel satisfies

$$\hat{f}_d^j = \frac{-\left(\left(\hat{\mathbf{v}}_u - \mathbf{v}_s^j \right) \cdot \mathbf{e}^j + \hat{t}_f - t_f^j \right) \cdot f_r}{c} \quad (9)$$

where $\mathbf{v}_s^j$ and t_f^j are the velocity vector and clock drift of the jth satellite, respectively; $\hat{\mathbf{v}}_u$ represents the user velocity vector which can be computed through the stand-lone vector GNSS SDR or the ultra-tight coupling receiver in this work; $\hat{t}_f$ stands for the local clock drift; c is the speed of light; $\mathbf{e}^j$ is the unit vector in the line-of-sight (LOS) direction; f_r denotes the GNSS radio frequency. More detailed introductions can be referred to [8]. In addition, the integration process of the proposed UTC architecture is implemented in the ECEF frame, while the position, velocity, and attitude (PVA) results are commonly computed in the local level frame (LLF) for analysis. As described in [15], the respective three-dimensional coordinates in ECEF frame have the access to be transferred as the latitude $\hat{L}_b$, longitude $\hat{\lambda}_b$, and height $\hat{h}_b$, in the LLF, i.e., $\mathbf{r}^n = \left[\hat{L}_b, \hat{\lambda}_b, \hat{h}_b\right]^{\mathrm{T}}$. The attitude matrix with respect to the rotation from the e-frame to the LLF can be attained as

$$\mathbf{C}_e^n = \begin{bmatrix} -\sin\hat{\lambda}_b & -\sin\hat{L}_b\cos\hat{\lambda}_b & \cos\hat{L}_b\cos\hat{\lambda}_b \\ \cos\hat{\lambda}_b & -\sin\hat{L}_b\sin\hat{\lambda}_b & \cos\hat{L}_b\sin\hat{\lambda}_b \\ 0 & \cos\hat{L}_b & \sin\hat{L}_b \end{bmatrix}^{\mathrm{T}} \quad (10)$$

Hence, the estimated velocity vector in the e-frame can be transferred to the one in the LLF, or east-north-up (ENU) frame in this work, which can be computed as

$$\mathbf{v}^n = [v^e, v^n, v^u]^T = \mathbf{C}_e^n \mathbf{v}^e \tag{11}$$

III. Work Process of The Proposed UTC GNSS/INS Integration System

The work process of the proposed ultra-tight coupling algorithm is summarized in Figure 1. Firstly, the GNSS measurements are produced through the acquisition, tracking and measurement extraction implementations. Then, the pseudo-range and the Doppler measurements are used to compute the positioning and velocity solutions, respectively. The commonly used least square (LS) method is chosen here to compute the positioning, velocity, and timing (PVT) solutions in the GNSS software-defined receiver (SDR) developed in this research. After that, a blunder-check module #1 is used to examine the outliers in the navigation solutions. When the blunder check #1 is passed, the results will be allowed to combine with the INS mechanization solutions and an integration result will be output through the data fusion implementation. Otherwise, the scalar tracking (ST) will replaced of the vector tracking. Once the integrated solutions are obtained, they will pass another checking module, i.e., Blunder Check #2. If these computation solutions manage to pass its decision-making, the integration velocities instead of the velocities produced by the stand-alone GNSS SDR would subsequently be used to update the Doppler information to aid the carrier NCO. If they fail to pass the Blunder Check #2, the ultra-tight coupling GNSS SDR will turn to the vector-tracking GNSS SDR.

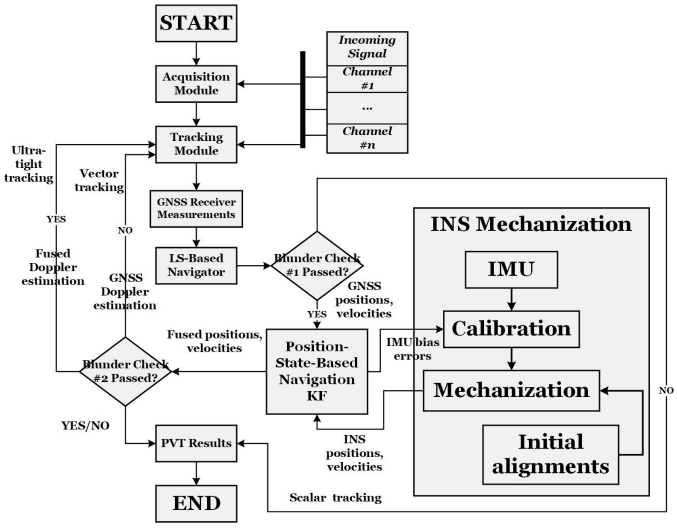

Fig. 1. Work process of the proposed ultra-tightly coupled GNSS/consumer-level IMU integration navigation system.

IV. Field Test Results and Testing Trajectory

The field tests are implemented to verify the performance of the proposed UTC GNSS/INS integration navigation system. The GPS L1 C/A signals are processed by the GNSS SDR in this work.

A. Setup for Field Tests

The setup for the field test of the proposed UTC GNSS/INS integration navigation system are illustrated in Figure 2. The GNSS receiver front-end and the commercial U-Blox receiver were receiving the incoming GNSS signals using the same NovAtel antenna through a splitter. The GPS L1 C/A signals are tested and compared in the experiments. Then, the IMU data including the angular rates and the accelerations along the three directions are produced by the respective gyro and accelerometer sensors integrated in the one type of the Android smartphone, i.e., HUAWEI Mate 9, and they are collected through an installed application in the operated system (OS), i.e., AndroSensor. The initial aligned attitudes can also be known through AndroSensor such that the initial alignment process is omitted in this experiment. It is not the main research direction for this paper. The coherent integration length is 5ms, the feedback rate of the vector tracking and ultra-tight coupling is 5Hz, and the phase lock loop (PLL) bandwidth is 5Hz and 18Hz for vector tracking and scalar tracking, respectively. The re-acquistion algorithm is not used in the experiment. More parameter settings can refer to [8]. Finally, the Trimble R10 Receiver provides the reference trajectory in this research.

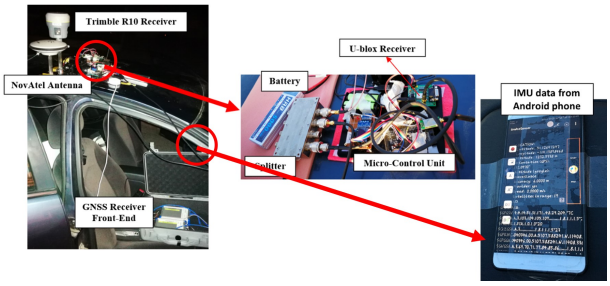

Fig. 2. Setup for the field test.

There are eighteen bridges in the field test. The testing scenario is an extremely challenging environment for GNSS navigation where the GNSS signals will be frequently interfered by different blockages. More detailed descriptions for the testing trajectory can refer to [8].

B. Experiment Results and Discussions

Figure 3 exhibits the C/N_0 estimations of all the visible satellites in terms of both vector tracking and ultra-tight coupling algorithms in the field tests, where all the incoming GNSS signals suffer from the frequent short-time blockages caused by the bridges in the testing trajectory as given in [8]. SV24 and SV32 embrace the worst performances in signal strength since their elevation angles are lowest among all the available satellites. However, the tracking channels of these two satellites are sufficiently robust against such extremely challenging environments in the full field tests based on these two algorithms. The sky plot is provided in Figure 4 as well.

The in-phase sample estimations corresponded to the VT- and UTC-based GNSS SDRs are illustrated in Figure 5

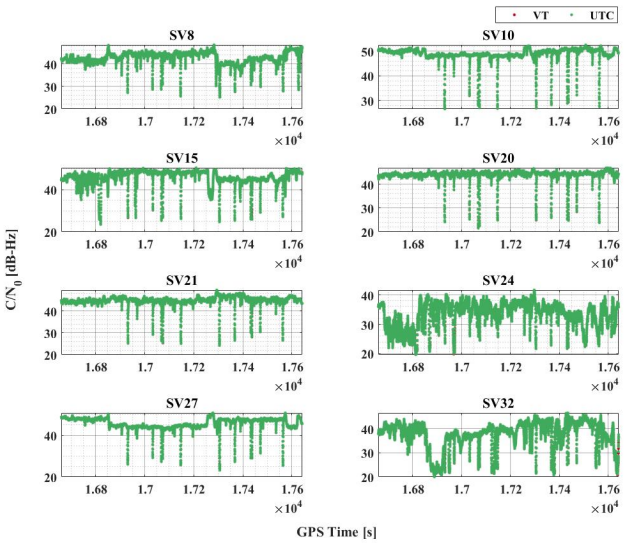

Fig. 3. C/N_0 estimations.

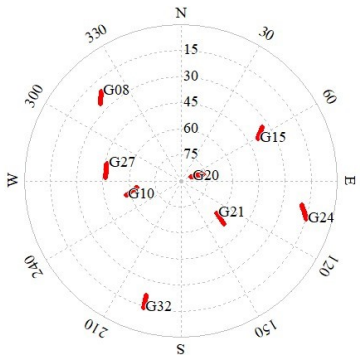

Fig. 4. Sky plot of the field test.

which shows the tracking-level performances. According to the results, in most of the cases, the ultra-tight receiver recovers from the signal fading within a shorter time than the counterpart in terms of the vector receiver. More specifically, the former instead of the vector tracking has a higher potential to re-demodulate the data bit after the interference in a more prompt way. Besides that, both the means and STDs of the carrier phase discriminator outputs are plot in Figure 6. In comparison with the results related to the VT GNSS SDR, most of the channel means estimated based on the ultra-tight algorithm have been largely improved except for the SV8 and SV21. The signal strengths of these two incoming signals are over 40 dB-Hz in most of the time during the test as provided in Figure 3. It implies that UTC GNSS/consumer-level low-cost IMU is very promising to further improve the tracking accuracy of weak channels but may inversely reduce the performances of the ones whose C/N_0 outputs are in good conditions. On the other hand, all the STDs estimated based on the UTC algorithms have been slightly increased compared with the VT methods. In other words, the increased spectrum power of the discriminator random noise should be closer to the real ones of the incoming signals except for SV8 and SV21. The overall positioning and navigation performance will be subsequently verified based on the RTK positioning algorithms. The open-source RTKLIB will be used to implement the high-precision positioning algorithms [17].

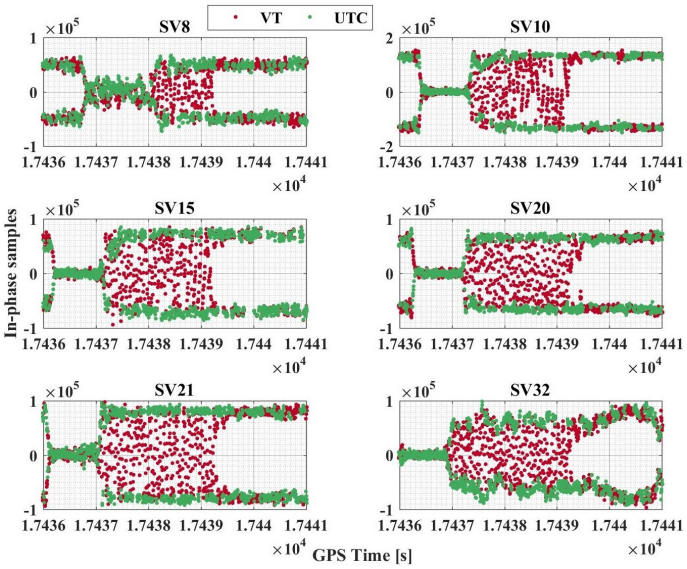

Fig. 5. In-phase sample estimations.

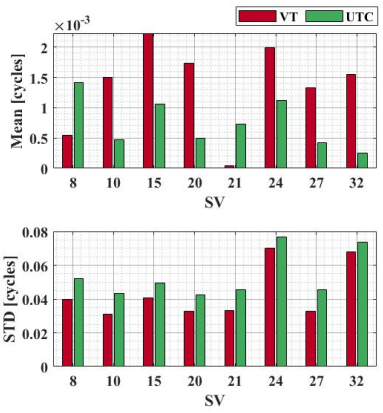

Fig. 6. Means (top) and STDs (bottom) of the carrier discriminating estimations.

As to the attitude estimations, it should be mentioned that the positive directions for pitch, roll, and azimuth are upwards, rolling to right, and from north direction clockwise, respectively. Both UTC and LC results are provided in Figure 7 where the GNSS SDR of the LC integration system is based on the vector tracking algorithm. As we can see, the pitch and roll estimations are both close to zeros. Then, referring to the test trajectory given in [8] and the estimated azimuth results, it can be inferred that the integration process and the related outputs are correct. In addition, it is also worth knowing that the attitude estimations between the UTC and VT-based LC architectures are very close to each other in this work.

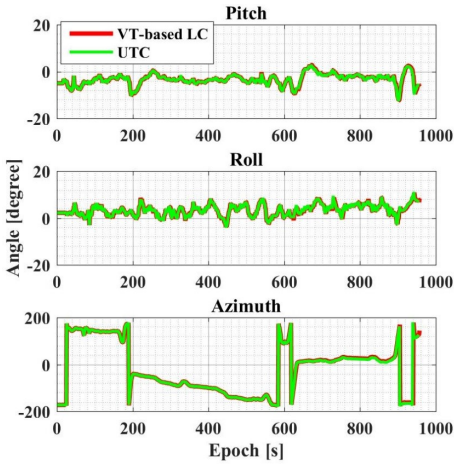

Fig. 7. Attitude estimations.

The performances of the carrier phase measurement processed by different methods are evaluated and compared with each other in Figure 8. Similarly, the RTK positioning results in terms of the VT- and UTC-aided GNSS SDR are computed using the RTKLIB software. On the one hand, both the two architectures manage to tolerate the extremely challenging environment for the full field-test time. In other words, it is shown that the continuous positioning solutions are provided with such two types of GNSS SDR over the experiment. On the other hand, there are still some discrepancies between these two. For example, the UTC-aided GNSS SDR can be recovered from some signal attenuated cases in a shorter time than the VT-aided GNSS SDR. Some tested results are given in Figure 8 to verify that the UTC architecture outperforms the VT system when the autonomous ground vehicle is confronted with the signal masking. When the car is just passing through a bridge, more available RTK solutions can be provided using the SDR with the proposed algorithm while the VT SDR needs more time to smooth the carrier phase measurement and, then, output the reliable observations.

Finally, the RTK positioning errors in the three directions are plot in Figure 9. The reference positioning solutions are produced by the Trimble R10 receiver. The positioning accuracies with respect to the different GNSS architectures are summarized in Table I. The availability percentage of the GNSS receiver has been significantly enhanced by the VT and UTC methods when such performances are compared with the one obtained from the ST SDR without using the re-acquisition algorithm. Meanwhile, the percentage related to the UTC is also higher than the one of VT, i.e., 99.3% versus 97.9%. In addition, the UTC-aided GNSS SDR performs slightly better than the commercial U-Blox receiver which embraces the availability percentage of 98.0%. The performance of the VT-aided GNSS SDR is very similar to the one of the U-Blox receiver in availability comparison, but they are both proved to be worse than the UTC-aided GNSS SDR. Since the filters used in the U-Blox's tracking loop are expected to be more optimized than the ones adopted in our GNSS SDR, it will

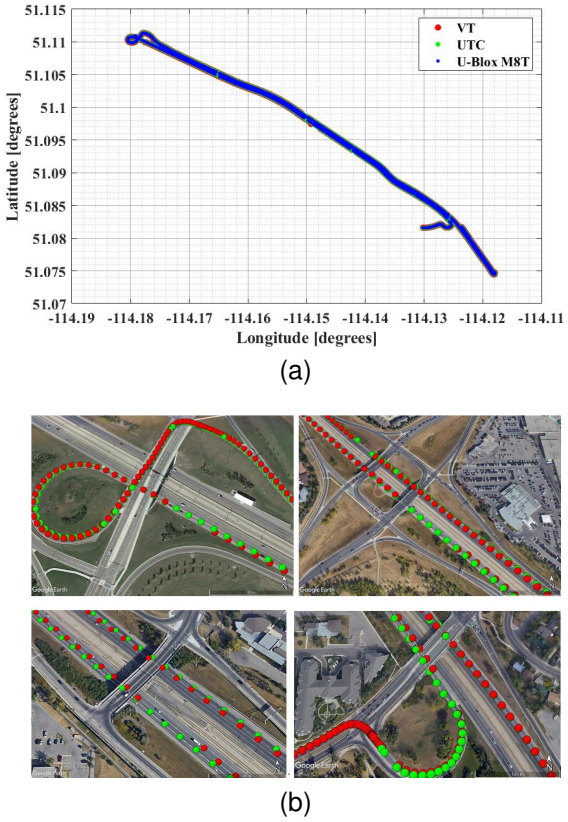

Fig. 8. RTK positioning estimations and the zoomed-in results in terms of vector-tracking and ultra-tight coupling GNSS SDRs.

take less time for the tracking channel of the U-Blox to be converged from the external interference. In this case, fewer outliers are supposed to be produced by the RTK positioning process in the U-Blox receiver solutions. All these analyses make it reasonable that the RTK positioning accuracy of the U-Blox receiver outperforms the proposed UTC- or VT-aided GNSS receiver.

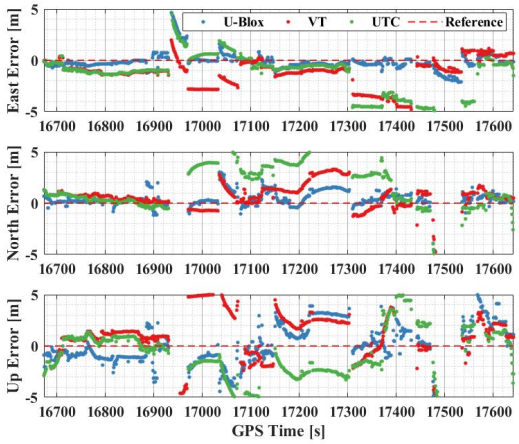

Fig. 9. RTK positioning estimation errors.

TABLE I
SUMMARIES OF THE RTK POSITIONING RESULTS IN TERMS OF DIFFERENT RECEIVER ARCHITECTURES.

Receiver Type	Availability			RMSE (RTKLIB RTK)		
	Epoch Number	Unavailable Points	Availability Percentage	East	North	Up
ST SDR	970s	711s	26.7%	N/A	N/A	N/A
VT SDR		20s	97.9%	0.680m	1.085m	1.808m
UTC SDR		7s	99.3%	0.623m	1.337m	1.815m
U-Blox		19s	98.0%	0.394m	0.785m	1.754m

V. CONCLUSIONS

An ultra-tightly coupled GNSS/INS integration navigation system using the consumer-level IMU data is proposed in this paper, and the performance of it is evaluated and compared with the loosely coupled VT-based GNSS/INS integration system and one type of the commercial receivers, i.e., U-Blox M8T. An extremely challenging environment for the GNSS receiver design is chosen as the field test scenario in this work. It is well-known that the U-Blox shows a strong power to offer customers with more self-contained, higher-performance, and lower-cost GNSS receiver, in the massive commercial market. In other words, the overall tracking performance in terms of the U-Blox receiver should be more optimized than the GNSS SDR used in this work. Many optimizing algorithms are neglected in the SDR since they are not the main contribution in the research. Thus, the fact that the RTK positioning accuracy of the U-Blox receier is higher than the proposed UTC- and VT-aided GNSS SDR is reasonable and acceptable. Meanwhile, the RTK positioning accuracies of the UTC- and VT-aided GNSS SDR are very close to each other. On the other hand, the experiment results in terms of the UTC-aided GNSS SDR are verified to outperform both the VT-based GNSS SDR and the U-Blox receiver in terms of the availability performance. The respective availability percentage of the UTC, VT LC, and the U-Blox are 99.3%, 97.9%, and 98.0%. The setup in terms of the smartphone and the GNSS antenna is not so accurate in the experiment. Besides that, the time synchronization problem is ignored in the implementation, and just the GPS time is used to synchronize the GNSS and IMU data in the fusion process. In this case, the performance of the proposed ultra-tightly coupled GNSS/INS integration system can be further improved once the mentioned issues can be solved. Furthermore, the analysis of the comparisons related to the various grade IMUs will be covered in the future works.

ACKNOWLEDGMENT

This work was supported in part by the National Natural Science Foundation of China under Grant 31727901, and in part by the Chang Jiang Scholars Programme under Grant T2012122.

REFERENCES

[1] J. J. Spilker Jr, *Global Positioning System: Theory And Applications, Volume 1, Chapter 7*. Washington D.C., USA: American Institute of Aeronautics and Astronautics, Inc., 1996.

[2] R. E. Phillips and G. T. Schmidt, "GPS/INS Integration," *AGARD Lecture Series MSP LS 207 on System Implications and Innovative Application of Satellite Navigation, NATO, Paris, July*, pp. 1–9, 1996.

[3] M. Petovello and G. Lachapelle, "Comparison of Vector-Based Software Receiver Implementations With Application to Ultra-Tight GPS/INS Integration," in *Proceedings of the 19th International Technical Meeting of the Satellite Division of The Institute of Navigation (ION GNSS 2006)*, Fort Worth, TX, USA, September 2006, pp. 1790–1799.

[4] M. Lashley, "Modelling and performance analysis of GPS vector tracking algorithms," Ph.D. Thesis, Auburn University, 2009.

[5] Y. Luo, L. Zhang, and H. Ruan, "An Acquisition Algorithm Based on FRFT for Weak GNSS Signals in A Dynamic Environment," *IEEE Communications Letters*, vol. 22, no. 6, pp. 1212–1215, 2018. [Online]. Available: https://ieeexplore.ieee.org/document/8344115/

[6] Y. Luo, L. Zhang, and N. El-Sheimy, "An improved DE-KFL for BOC signal tracking assisted by FRFT in a highly dynamic environment," in *Proceedings of IEEE/ION PLANS 2018*, Monterey, CA, USA, April 2018, pp. 1525–1534. [Online]. Available: https://ieeexplore.ieee.org/document/8373547/

[7] Y. Luo, C. Yu, S. Chen, J. Li, H. Ruan, and N. El-Sheimy, "A Novel Doppler Rate Estimator Based on Fractional Fourier Transform for High-Dynamic GNSS Signal," *IEEE Access*, vol. 7, pp. 29 575–29 596, 2019. [Online]. Available: https://ieeexplore.ieee.org/document/8660391/

[8] Y. Luo, J. Li, C. Yu, Z. Lyu, Z. Yue, and N. El-Sheimy, "A GNSS Software-Defined Receiver with Vector Tracking Techniques for Land Vehicle Navigation," in *Proceedings of the ION 2019 Pacific PNT Meeting*, Honolulu, Hawaii, USA, April 2019, pp. 713–727. [Online]. Available: https://www.ion.org/publications/abstract.cfm?articleID=16834

[9] B. Xu and L.-T. Hsu, "NLOS Detection and Compensation using a Vector Tracking-based GPS Software Receiver," in *Proceedings of the ION 2019 Pacific PNT Meeting*, Honolulu, Hawaii, USA, April 2019, pp. 702–712. [Online]. Available: https://www.ion.org/publications/abstract.cfm?articleID=16777

[10] Y. Luo, J. Li, C. Yu, B. Xu, Y. Li, L.-T. Hsu, and N. El-Sheimy, "Research on Time-Correlated Errors Using Allan Variance in a Kalman Filter Applicable to Vector-Tracking-Based GNSS Software-Defined Receiver for Autonomous Ground Vehicle Navigation," *Remote Sensing*, vol. 11, no. 9, p. 1026, 2019. [Online]. Available: https://www.mdpi.com/2072-4292/11/9/1026

[11] S. Daneshmand and G. Lachapelle, "Integration of GNSS and INS with a phased array antenna," *GPS Solutions*, vol. 22, no. 1, pp. 1–14, 2018.

[12] Y. Li, S. Zahran, Y. Zhuang, Z. Gao, Y. Luo, Z. He, L. Pei, R. Chen, and N. El-Sheimy, "IMU/Magnetometer/Barometer/Mass-Flow Sensor Integrated Indoor Quadrotor UAV Localization with Robust Velocity Updates," *Remote Sensing*, vol. 11, no. 7, p. 838, 2019. [Online]. Available: https://www.mdpi.com/2072-4292/11/7/838

[13] M. Moussa, A. Moussa, and N. El-Sheimy, "Steering Angle Assisted Vehicular Navigation Using Portable Devices in GNSS-Denied Environments," *Sensors*, vol. 19, no. 7, p. 1618, 2019. [Online]. Available: https://www.mdpi.com/1424-8220/19/7/1618

[14] D. Wang, Y. Lu, L. Zhang, and G. Jiang, "Intelligent Positioning for a Commercial Mobile Platform in Seamless Indoor/Outdoor Scenes based on Multi-sensor Fusion," *Sensors*, vol. 19, no. 7, p. 1696, 2019. [Online]. Available: https://www.mdpi.com/1424-8220/19/7/1696

[15] P. D. Groves, *Principles of GNSS, inertial, and multisensor integrated navigation systems*, 2nd ed. Artech house, 2013.

[16] R. G. Brown and P. Y. C. Hwang, *Introduction to random signals and applied Kalman filter with Matlab exercises*, 4th ed. Hoboken: Wiley, 2012.

[17] T. Takasu and A. Yasuda, "Development of the low-cost RTK-GPS receiver with an open source program package RTKLIB," in *Proceedings of the International symposium on GPS/GNSS*, Jeju, Korea, November 2009.